Composites Part B 150 (2018) 234–241

Contents lists available at ScienceDirect

Composites Part B

journal homepage: www.elsevier.com/locate/compositesb

Facile synthesis of porous $CuCo_2O_4$ composite sheets and their supercapacitive performance

Ashok Kumar Das[a,c], Nam Hoon Kim[b], Seung Hee Lee[a], Youngku Sohn[c,**], Joong Hee Lee[a,b,*]

[a] Advanced Materials Institute for BIN Convergence Technology (BK21 Plus Global Program), Department of BIN Convergence Technology, Chonbuk National University, Jeonju, Jeonbuk 54896, Republic of Korea

[b] Carbon Composite Research Center, Department of Polymer-Nano Science and Technology, Chonbuk National University, Jeonju, Jeonbuk 54896, Republic of Korea

[c] Department of Chemistry, Chungnam National University, Daejeon 34134, Republic of Korea

ARTICLE INFO

Keywords:
Nano-structures
Interface
Chemical properties
Electron microscopy

ABSTRACT

The synthesis of metal oxide composites with porous structures for supercapacitor application has drawn much attention owing to their high surface area and easy access of the electrolyte ions to the electrode surface through the pores of the active materials. A facile hydrothermal approach is suggested for the synthesis of porous $CuCo_2O_4$ composite sheets and their application as an active electrode material for supercapacitor application. Field emission scanning electron microscopy (FESEM) and transmission electron microscopy (TEM) measurements show the formation of porous $CuCo_2O_4$ composite sheets. BET surface area measurements show that the porous $CuCo_2O_4$ composite sheet has 69.44 $m^2 g^{-1}$ surface area, which is 4.7 times higher than quasi-spherical $CuCo_2O_4$ nanoparticles. The porous $CuCo_2O_4$ composite sheet delivered 1037 $C g^{-1}$ specific capacity at 5 $mV s^{-1}$. Additionally, the porous $CuCo_2O_4$ composite sheet retained 94% of its initial specific capacity after 5000 charge-discharge cycles at 10 $A g^{-1}$ indicating an excellent cyclic stability. This excellent supercapacitive performance is attributed to the high surface area and enhanced ion transport through the pores of the $CuCo_2O_4$ sheets. This high specific capacity and excellent cyclic stability of the porous $CuCo_2O_4$ composite sheets prove to be a promising candidate for supercapacitor application.

1. Introduction

The increasing energy requirement and global warming arising owing to the substantial use of fossil fuels has triggered the extensive research interest towards the generation of sufficient amount of energy in cleaner method [1–13]. In this regard, development of various high-performance energy storage devices, such as fuel cells, batteries, and supercapacitors has gained enormous attention in recent years [14]. Among the aforementioned energy storage devices, much attention has been paid towards the development of high-performance supercapacitors to meet the future energy demand, as they have several advantages, including fast charging and discharging ability, longer cyclic lifespans, and wide operating temperature ranges over the fuel cell and battery [15]. In supercapacitors, charge-storage occurs either by ion adsorption or redox reactions and this mechanism of charge-storage categorizes them into electrical double layer capacitors (EDLCs) and pseudocapacitors, respectively [16]. The pseudocapacitors fabricated using transition metal oxides deliver high specific capacitance than the EDLCs [17]. But, the poor conductivity of transition metal oxides leads to low specific capacitance, thereby hindering their utilization in the development of high performance energy storage devices. Conversely, mixed transition metal oxide spinels containing two different metal atoms show two times higher electronic conductivity and electrochemical performance compared to their individual single metal oxides [16]. Owing to these superior physiochemical properties, mixed transition metal oxide spinels have emerged as the potential candidate for the fabrication of high performance supercapacitors [18]. For instance, mixed transition metal oxide spinels, $CoFe_2O_4$ [19], $ZnFe_2O_4$ [20], $CuFe_2O_4$ [21], $NiFe_2O_4$ [22] $CoMn_2O_4$ [23], $NiMn_2O_4$ [24], $ZnMn_2O_4$ [25], etc., have been used in the fabrication of supercapacitor. In recent years, low cost cobaltite spinels, such as $NiCo_2O_4$ [26], $MgCo_2O_4$ [27], $ZnCo_2O_4$ [28], $FeCo_2O_4$ [29], $MnCo_2O_4$ [30] and $CuCo_2O_4$ [31] etc are emerged as the another class of active material for supercapacitor application. Among these cobaltite spinels, synthesis of $CuCo_2O_4$ has drawn much attention, because it has excellent potential in the area of electrocatalysis [32], Li-ion batteries [33], and

* Corresponding author. Advanced Materials Institute for BIN Convergence Technology (BK21 Plus Global Program), Department of BIN Convergence Technology, Chonbuk National University, Jeonju, Jeonbuk 54896, Republic of Korea.

** Corresponding author.

E-mail addresses: youngkusohn@cnu.ac.kr (Y. Sohn), jhl@chonbuk.ac.kr (J.H. Lee).

https://doi.org/10.1016/j.compositesb.2018.05.028
Received 3 April 2018; Received in revised form 11 May 2018; Accepted 21 May 2018
Available online 28 May 2018

supercapacitors [34] owing to its two times higher performance than either single component copper oxide or cobalt oxide [32]. As per the performance of supercapacitors is concerned, it is intensely reliant on the morphology, surface area and porosity of the active electrode material used in its fabrication [1,31]. In principle, by regulating the surface morphology, surface area and porosity of $CuCo_2O_4$, the performance of $CuCo_2O_4$ based supercapacitor could also be easily regulated.

Considering the aforementioned facts and taking account the importance of $CuCo_2O_4$ in the area of supercapacitor fabrication, in the current investigation, we have attempted for the synthesis of porous $CuCo_2O_4$ sheets and their supercapacitive performance has been demonstrated. To the best of our knowledge, this is the first report on the hydrothermal synthesis of porous $CuCo_2O_4$ sheets for supercapacitor application. The porous $CuCo_2O_4$ sheets exhibited excellent electrochemical performances in terms of specific capacity, rate capability, and cyclic stability. The excellent supercapacitive performance of the porous $CuCo_2O_4$ sheets could be attributed to its unique porous morphology which facilitated the electrolyte access as well as enhanced the electron transport.

2. Experimental

2.1. Materials

$CuCl_2{\cdot}6H_2O$, $CoCl_2{\cdot}6H_2O$, polyvinylidene fluoride (PVDF) and activated carbon were purchased from Sigma-Aldrich (Germany) and were used as received. Ammonium hydroxide, N-methyl-2-pyrrolidone (NMP) and potassium hydroxide were purchased from Samchun Pure Chemical Co. Ltd. (Korea). For electrochemical measurements 6 M KOH was used as supporting electrolyte. Millipore water (Milli-Q system) was used for the preparation of solutions.

2.2. Synthesis of porous $CuCo_2O_4$ composite sheets

Porous $CuCo_2O_4$ sheets were synthesized by hydrothermal method and is represented in Scheme 1. Typically, 10 mM of $CuCl_2{\cdot}6H_2O$ and 20 mM of $CoCl_2{\cdot}6H_2O$ were dissolved in 50 mL of DI water through continuous stirring for 30 min. A desired volume of ammonium hydroxide was added to this solution drop by drop till the pH of the solution becomes 14 and the mixture was further stirred for additional 30 min. Then the whole solution was transferred into a 100 mL Tefon-lined stainless steel autoclave and subjected for hydrothermal treatment at 180 °C for 24 h. After completion of the hydrothermal reaction, the autoclave was cooled down to room temperature and the Cu–Co hydroxide precursor was collected through filtration followed by repeated washing in water and ethanol.

The obtained Cu–Co hydroxide precursor was dried at 60 °C for 12 h. Finally, the as-synthesized Cu–Co hydroxide precursor was annealed in air for 4 h at 400 °C at a ramping rate of 2 °C min^{-1} to obtain porous $CuCo_2O_4$ composite sheets. For comparative study, quasi-spherical $CuCo_2O_4$ nanoparticles were synthesized according to a method described in the reported literature [35].

2.3. Characterization

The Fourier transform infrared (FTIR) spectra were recorded using a Thermo Scientific Nicolet iS10 spectrometer with a diamond crystal based attenuated total reflectance mode. The X-ray diffraction (XRD) patterns were recorded using a powder PANalytical X'Pert Pro MPD X ray diffractometer with a Cu-Kα target (λ = 1.5406 Å). The Raman spectra were recorded using a Nanofinder 30 system (Tokyo Instruments Co., Osaka, Japan). The Brunauer-Emmett-Teller (BET) surface area was measured using Micromeritics Tristar 3000 analyzer. The morphology analysis was carried out using a field emission scanning electron microscope (SUPRA40VP, Carl Zeiss, Germany). The transmission electron microscopic (TEM) images and high-resolution transmission electron microscopic (HR-TEM) images were recorded using a field emission transmission electron microscope (FE-TEM; JEOL JEM-2200 FS, Japan). The TEM sample was prepared by dispersing the sample (0.1 mg/mL) in ethanol by ultrasonication, and 5 μL of the dispersion was drop-casted on a carbon coated Ni grid. The electrochemical measurements were performed using a Zive-SP1 electrochemical workstation (Wonatech, Korea) in a three-electrode

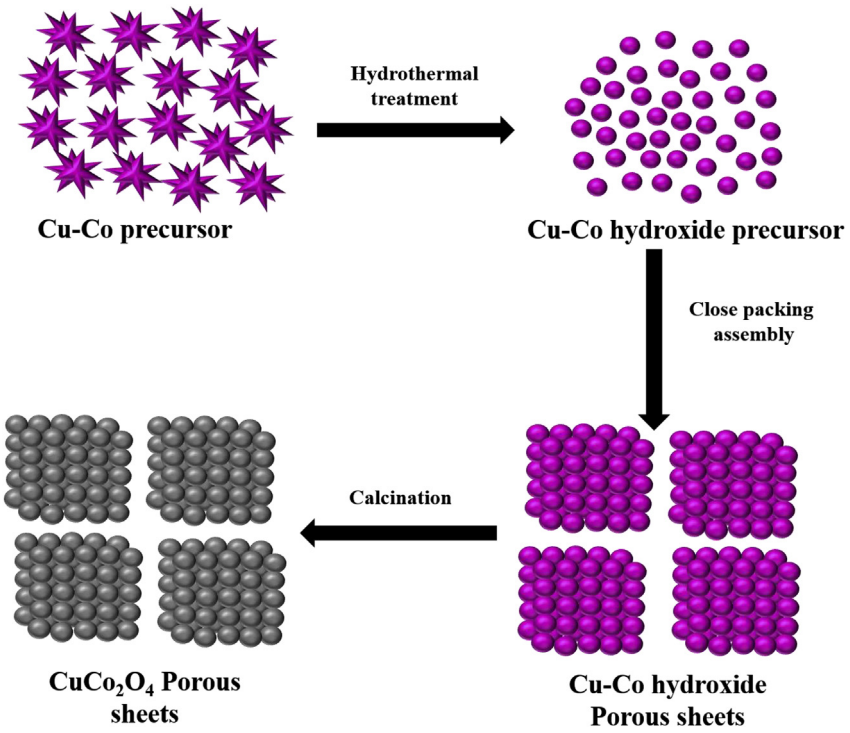

Scheme 1. Scheme displaying the synthesis of porous $CuCo_2O_4$ composite sheet.

configuration where carbon paper (CP, dimension 1 cm × 2 cm) containing either porous $CuCo_2O_4$ composite sheet or $CuCo_2O_4$ quasi-spherical nanoparticles, Pt wire, and Ag/AgCl (3 M NaCl) were used as the working, counter, and reference electrodes, respectively. The working electrodes were fabricated by drop casting of $CuCo_2O_4$ sample slurries on the CP substrate within a 1 cm × 1 cm area. The slurries were prepared by grinding 6, 2 and 2 mg of either porous $CuCo_2O_4$ sheet or $CuCo_2O_4$ quasi-spherical nanoparticles, PVDF and activated carbon, respectively, in 2 mL NMP solvent. From the slurries, initially a 100 µl was pipetted out and drop casted over the CP substrate followed by drying at 60 °C for 1 min. This process was continued till all the slurries get deposited over the CP substrate and allowed for overnight drying at 60 °C to achieve $CuCo_2O_4$ based working electrodes All electrochemical experiments were performed using 6 M KOH as electrolyte.

3. Results and discussion

3.1. Characterization of quasi-spherical and porous $CuCo_2O_4$ composite sheets

3.1.1. XRD analysis

The as-prepared quasi-spherical $CuCo_2O_4$ composite nanoparticles and porous $CuCo_2O_4$ composite sheets were characterized by X-ray diffraction (XRD) analysis and is shown in Fig. 1. The XRD profile of quasi-spherical $CuCo_2O_4$ composite nanoparticles and porous $CuCo_2O_4$ composite sheets shows the presence of nine peaks corresponding to the (111), (220), (311), (222), (400), (422), (511), (440) and (533) plane reflections of the spinel $CuCo_2O_4$ crystalline structure, suggesting the formation of $CuCo_2O_4$ spinel. In both cases, the (311) plane is highly intense compared to their other planes and in the case of porous $CuCo_2O_4$ composite sheets, the (311) plane has highest intensity than the quasi-spherical $CuCo_2O_4$ nanoparticles. Most importantly, in the XRD spectrums of quasi-spherical $CuCo_2O_4$ nanoparticles and porous $CuCo_2O_4$ sheets no signatures for CuO, CoO, CoO2 and Co were found suggesting that the prepared samples are highly pure [15].

3.1.2. FTIR analysis

The as-synthesized quasi-spherical $CuCo_2O_4$ nanoparticles and porous $CuCo_2O_4$ composite sheets were further characterized by FTIR measurement and their FTIR profile is represented in Fig. 2. The $CuCo_2O_4$ spinel is known to show two sharp bands within 400 and 700 cm^{-1}. Interestingly, in the current case, both the spectrums show the presence of two intense bands at 554 and 648 cm^{-1}, corresponding to the stretching vibration of Co^{3+}-O^{2-} in the tetrahedral complexes and Cu^{2+}-O^{2-} in the octahedral complexes, respectively [36]. Since in the spectrum of $CuCo_2O_4$ composite samples two sharp bands were noticed within 400 and 700 cm^{-1}, therefore, the synthesized product is pure $CuCo_2O_4$ spinel [37].

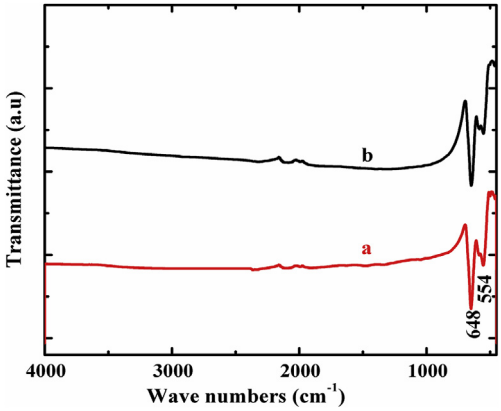

Fig. 2. FTIR spectra of (a) quasi-spherical $CuCo_2O_4$ nanoparticles and (b) porous $CuCo_2O_4$ sheet.

3.1.3. Raman analysis

The structural properties of the as-synthesized quasi-spherical $CuCo_2O_4$ nanoparticles and porous $CuCo_2O_4$ composite sheets were investigated by Raman measurement. Fig. 3 represents the Raman profile of quasi-spherical $CuCo_2O_4$ nanoparticles and porous $CuCo_2O_4$ sheets. Both $CuCo_2O_4$ composite samples have four distinct peaks at 187, 479.1, 524.7 and 678.3 cm^{-1}, corresponding to the F_{2g}, E_g, F_{2g} and A_{1g} modes of $CuCo_2O_4$ spinel, respectively. Signatures corresponding to the Co–O and Cu–O vibrations were visible, but no signature corresponding to the OH group was noticed, signifying that the Cu–Co hydroxide precursor has been entirely converted to $CuCo_2O_4$ spinel after calcination at 400 °C. The current Raman result is in well accordance with the result reported earlier [32].

3.1.4. BET analysis

The specific surface area and pore size distribution of the quasi-spherical $CuCo_2O_4$ nanoparticles and porous $CuCo_2O_4$ composite sheets were investigated by BET analysis as pores and surface area of the active material plays a significant role on the supercapacitive performance. Fig. 4 represents the BET profile of quasi-spherical $CuCo_2O_4$ nanoparticles and porous $CuCo_2O_4$ composite sheets which shows that both the samples have type IV isotherm with a type H3 hysteresis loop replication of the distinctive mesoporous structure [38]. The BET surface area of the quasi-spherical $CuCo_2O_4$ nanoparticles and porous $CuCo_2O_4$ composite sheets are measured to be 14.71 and 69.44 m^2g^{-1}, respectively. The surface area of the porous $CuCo_2O_4$ sheet is 4.7 times higher than the quasi-spherical $CuCo_2O_4$ nanoparticles. The higher BET

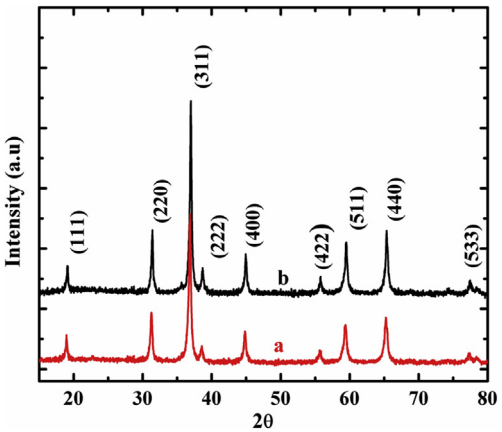

Fig. 1. XRD pattern of (a) quasi-spherical $CuCo_2O_4$ nanoparticles and (b) porous $CuCo_2O_4$ sheet.

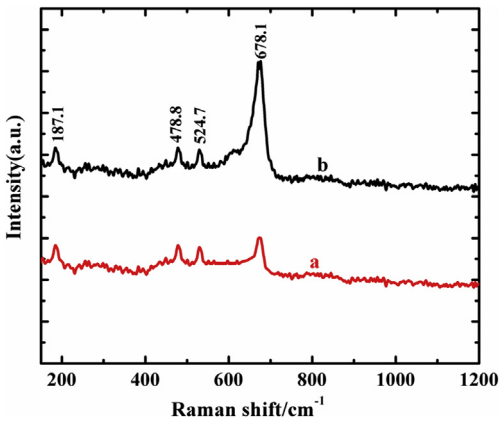

Fig. 3. Raman spectra of (a) quasi-spherical $CuCo_2O_4$ nanoparticles and (b) porous $CuCo_2O_4$ composite sheets.

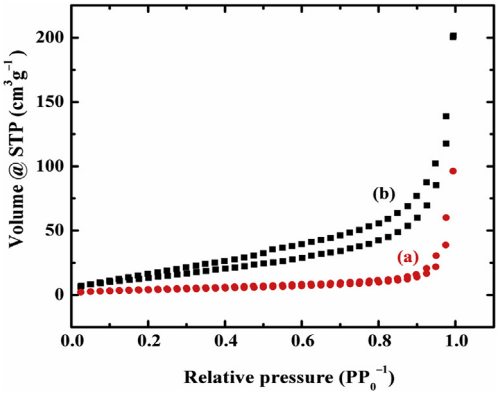

Fig. 4. BET isotherm of (a) quasi-spherical $CuCo_2O_4$ nanoparticles and (b) porous $CuCo_2O_4$ composite sheet.

surface area of the porous $CuCo_2O_4$ sheet could be attributed to its porous structure. The high surface area and high porosity of the active material is known to be beneficial for the high performance supercapacitors. Typically, porous $CuCo_2O_4$ with an appropriate conductivity is a potential candidate for the development high performance energy storage devices. In the present case, because of the porous structure, a large number of channels are expected to be present in the porous $CuCo_2O_4$ sheets for the efficient transport of electrolyte ions to the electrode surface owing to the reduced electrolyte flow tracks. At the same time, due to the high surface area, more interaction between active material and electrolyte is anticipated leading to faster redox reactions. The combined effect of porous nature and high surface area in turn could lead to the excellent electrochemical performance.

3.1.5. FESEM analysis

The morphology of the as-synthesized $CuCo_2O_4$ composite samples were investigated by SEM analysis and their SEM images are shown in Fig. 5. As can be seen in the Fig. 5a, the as-synthesized quasi-spherical $CuCo_2O_4$ nanoparticles have an average size of 100 nm. On the other hand the $CuCo_2O_4$ synthesized at our optimized experimental condition has porous sheet like morphology (Fig. 5b). The length and width of the porous $CuCo_2O_4$ sheet is not consistent, however, the thickness of each sheet is noticed to be ~ 5 nm. The high magnified SEM image of a single sheet (in set in Fig. 5b) shows that the porous $CuCo_2O_4$ sheets are composed quasi-spherical $CuCo_2O_4$ nanoparticles interconnected to each other. The close examination of the high magnified SEM image of the porous $CuCo_2O_4$ sheet clearly reveals that it has numerous pores in the middle of the interlinked quasi-spherical $CuCo_2O_4$ nanoparticles with a size ranging from ~10–20 nm. This special porous morphology of $CuCo_2O_4$ is quite favorable for the high performance supercapacitor application, as easy access of electrolyte ions is anticipated through the pores of the porous $CuCo_2O_4$ sheets.

3.1.6. TEM analysis

The microstructure and chemical composition of the quasi-spherical $CuCo_2O_4$ nanoparticles and porous $CuCo_2O_4$ composite sheets were investigated by TEM, HRTEM, selected area electron diffraction (SAED) and elemental mapping analysis and is represented in Fig. 6. As shown in Fig. 6a, quasi-spherical $CuCo_2O_4$ nanoparticles have an average size of 150 nm, whereas the single porous $CuCo_2O_4$ composite sheet (Fig. 6b) comprised of interconnection of many nanoparticles. The length and width of each porous $CuCo_2O_4$ composite sheet is found to be 300 and 250 nm, respectively. The high magnified TEM image (Fig. 6c) of a porous $CuCo_2O_4$ composite sheet shows that the size of the pores are ~ 10–20 nm. The HRTEM image (Fig. 6d) shows that the lattice fringes of $CuCo_2O_4$ composite sheet were 0.20, 0.242 and 0.468 nm, corresponding to the (400), (311) and (111) planes of spinel $CuCo_2O_4$, respectively [15,32]. The SAED pattern shows that it consists of several well-defined diffraction rings (Fig. 6e) indicating the polycrystalline nature of $CuCo_2O_4$ composite sheet. The diffraction rings are indexed to the (220), (311), (400) and (440) planes of the cubic $CuCo_2O_4$ phase, which are consistent with the XRD result. In order to further elucidate the chemical composition of porous $CuCo_2O_4$ composite sheet, the elemental mapping technique was applied to an individual porous $CuCo_2O_4$ composite sheet. The dark-field scanning transmission electron microscopic (DF-STEM) image of a porous $CuCo_2O_4$ sheet and its chemical composition signature is shown in Fig. 6f. As can be seen in Fig. 6f, it was observed that the elements Cu, Co, and O are uniformly distributed inside the $CuCo_2O_4$ spinel as porous sheet like structure, further supporting that the resulting porous sheet is composed of the elements Cu, Co, and O.

3.2. Supercapacitive property

The electrochemical performance of the porous $CuCo_2O_4$ composite sheets and quasi-spherical $CuCo_2O_4$ nanoparticles were investigated in 6 M KOH electrolyte using cyclic voltammetry (CV), galvanostatic charge-discharge (GCD) and electrochemical impedance spectroscopy (EIS) methods. Fig. 7 represents the voltammetric profile obtained on the porous $CuCo_2O_4$ composite sheet and quasi-spherical $CuCo_2O_4$ nanoparticle based electrode in the potential range from −0.2–0.6 V at a scan rate of 5 mV s^{-1}. In both cases, a pair of redox peaks, signature for battery-type electrode were noticed at ~ 0.178 V and ~ 0.371 V, revealing the pseudocapacitive nature of the as-synthesized $CuCo_2O_4$ materials. The evolution of the peaks is believed to have originated from the Faradic redox reaction related to the inter conversion of Co^{4+}/Co^{3+} and Cu^{2+}/Cu^{+} in alkaline medium [35].

These voltammetric profiles are quite different from the EDLCs which shows rectangular shaped voltammetric profiles. As can be seen in Fig. 7, the voltammetric profile obtained on the quasi-spherical $CuCo_2O_4$ nanoparticle based electrode has a small integral area than the porous $CuCo_2O_4$ sheet based electrode. Since, the porous $CuCo_2O_4$ composite sheets has a large integral area, therefore a high specific capacity is anticipated in this case, as specific capacity is related with

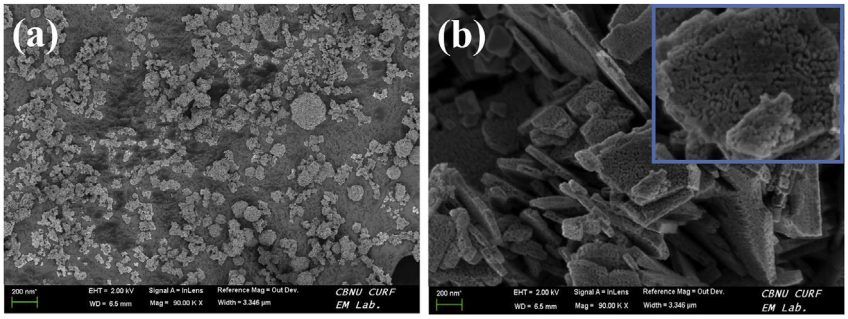

Fig. 5. FE-SEM image of (a) quasi-spherical $CuCo_2O_4$ nanoparticles and (b) porous $CuCo_2O_4$ composite sheet. The inset in Fig. 5(b) shows the high magnified image of a porous $CuCo_2O_4$ composite sheet.

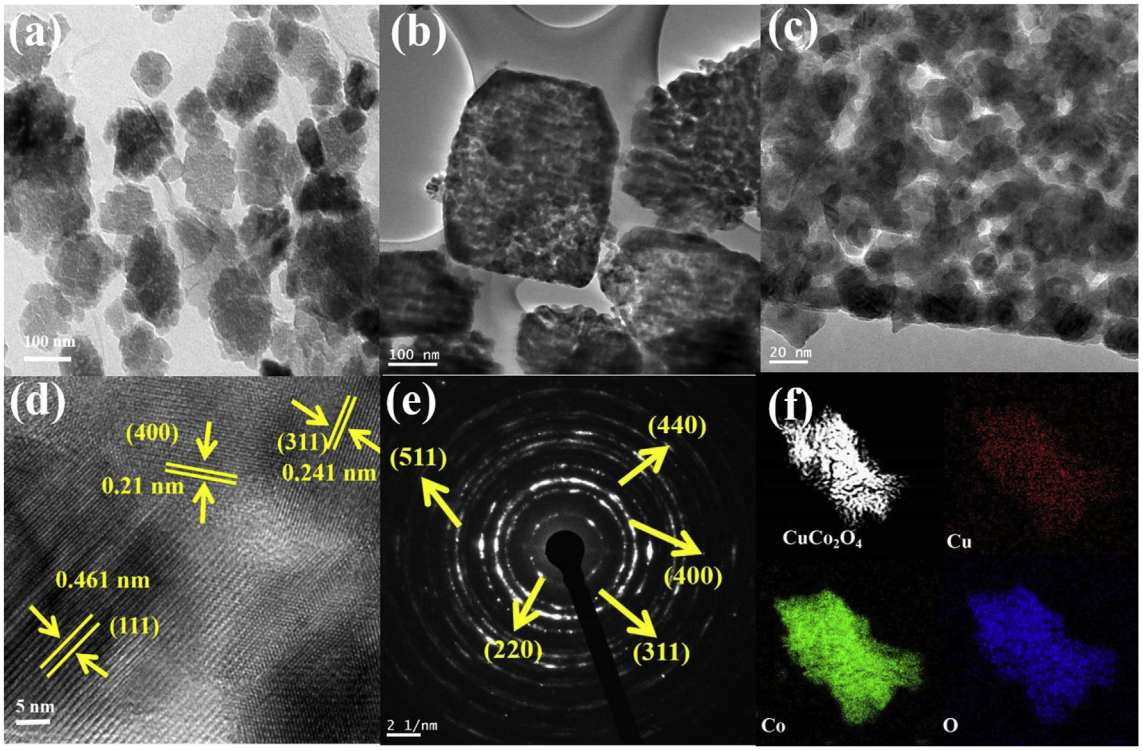

Fig. 6. TEM images of (a) quasi-spherical $CuCo_2O_4$ nanoparticles and (b) porous $CuCo_2O_4$ sheet. High magnified TEM image (c) and HRTEM image (d) of porous $CuCo_2O_4$ sheet. SAED pattern (e) and elemental mapping (f) of porous $CuCo_2O_4$ sheet.

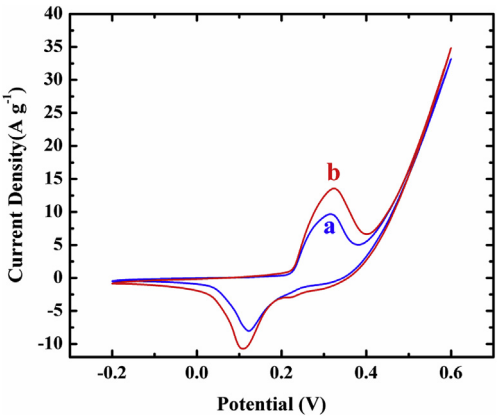

Fig. 7. Cyclic voltammograms of (a) quasi-spherical $CuCo_2O_4$ nanoparticles and (b) porous $CuCo_2O_4$ sheet based electrodes in 6 M KOH. Scan rate: 5 mV s^{-1}.

the integral area of the voltammetric profile [1]. The specific capacity of quasi-spherical $CuCo_2O_4$ nanoparticle and porous $CuCo_2O_4$ composite sheets based electrode was calculated following a reported method [39]. On the porous $CuCo_2O_4$ composite sheet based electrode, 1037 C g^{-1} specific capacity was obtained at 5 mV s^{-1}, whereas at the same scan rate, on the quasi-spherical $CuCo_2O_4$ nanoparticle based electrode 917 C g^{-1} specific capacity was obtained.

The specific capacity value of porous $CuCo_2O_4$ composite sheet is 1.13 times larger than that observed on quasi-spherical $CuCo_2O_4$ nanoparticle, indicating the superior supercapacitive performance of porous $CuCo_2O_4$ composite sheet. The scan rate impact on the performance of porous $CuCo_2O_4$ sheet and quasi-spherical $CuCo_2O_4$ nanoparticle was investigated at 5, 10, 20, 30, 40 and 50 mV s^{-1} scan rates. Fig. 8a, represents the voltammetric signature obtained on the porous $CuCo_2O_4$ composite sheet based electrode. The analysis of the shape of individual voltammograms clearly shows no such drastic change in

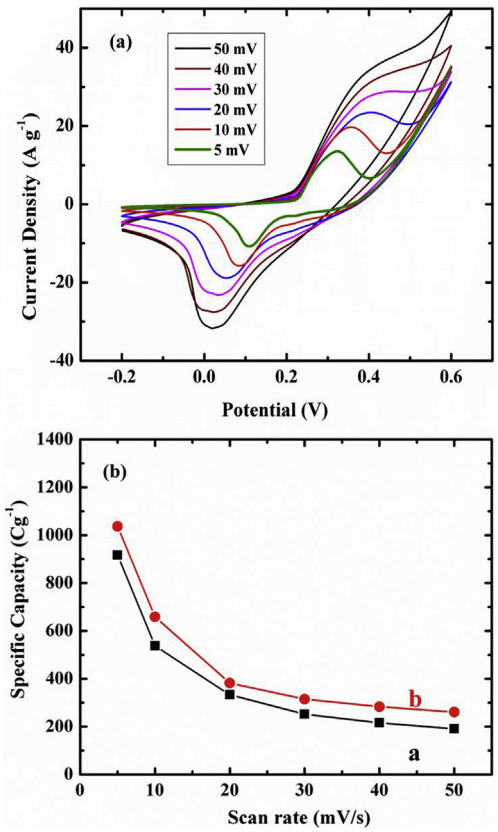

Fig. 8. (a) Cyclic voltammograms of porous $CuCo_2O_4$ composite sheet based electrode in 6 M KOH at various scan rates from 5 mV s^{-1} to 50 mV s^{-1} and (b) specific capacity dependent on scan rates of porous $CuCo_2O_4$ composite sheet based electrode.

their shape, except from the shifting in the oxidation and reduction peaks in positive and negative directions, respectively. The shifting in the peak position and shape preservation signifies the respective electrode polarization and exceptional reversibility which is vital for power devices. The same type of voltammetric behavior and profile was also noticed on the quasi-spherical $CuCo_2O_4$ nanoparticle based electrode (Fig. S1).

The plot of specific capacity as a function of scan rates is represented in Fig. 8b. The specific capacity value of porous $CuCo_2O_4$ composite sheet decreased with the increase in scan rate (Fig. 8b), because of the partial contact of porous $CuCo_2O_4$ composite sheet with OH^- ions in short time, whereas, in lower scan rate the inner and outer surface finds enough time for the interaction with OH^- ions resulting in a high specific capacity. On the quasi-spherical $CuCo_2O_4$ nanoparticle based electrode the specific capacity value followed the same trend as in the case of porous $CuCo_2O_4$ composite sheet. In all scan rate, porous $CuCo_2O_4$ composite sheet delivered highest specific capacity than the quasi-spherical $CuCo_2O_4$ nanoparticles.

The quasi-spherical $CuCo_2O_4$ nanoparticle has 191 $C\,g^{-1}$ specific capacity with 20% retention at 10 fold increase in the scan rate. Conversely, the same 10 fold increase in the scan rate the porous $CuCo_2O_4$ composite sheet delivered 261 $C\,g^{-1}$ specific capacity with 25% retention, which is 1.25 times larger than the quasi-spherical $CuCo_2O_4$ nanoparticles, suggesting its excellent supercapacitive performance. The performance of the porous $CuCo_2O_4$ composite sheet and quasi-spherical $CuCo_2O_4$ nanoparticle based electrodes were further investigated by the galvanostatic charge-discharge measurement in the potential window of -0.2–0.45 V at an applied current density of 2 $A\,g^{-1}$ and their respective GCD profile is represented in Fig. 9a. The GCD profiles in both cases differ from straight line, signifying that the charge storage is reigned by the Faradic reactions. The GCD profiles display voltage plateau at ~ 0.1 V, consistent with the voltammetric profile. Compared to the quasi-spherical $CuCo_2O_4$ nanoparticle, the porous $CuCo_2O_4$ composite sheet has longest discharge time indicating that on this electrode highest specific capacity could be achieved. The specific capacity value of the quasi-spherical $CuCo_2O_4$ nanoparticle and porous $CuCo_2O_4$ composite sheet was calculated from the galvanostatic charge-discharge profile following the method described elsewhere [39].

The specific capacity value obtained on the porous $CuCo_2O_4$ composite sheet based electrode at 2 $A\,g^{-1}$ current density was 449 $C\,g^{-1}$ which is 1.5 times larger than the quasi-spherical $CuCo_2O_4$ nanoparticle (320 $C\,g^{-1}$), indicating the excellent supercapacitive performance of porous $CuCo_2O_4$ composite sheets (Fig. 9b). To understand the link between applied current densities and specific capacity, GCD profiles of quasi-spherical $CuCo_2O_4$ nanoparticle and porous $CuCo_2O_4$ composite sheets were recorded at different applied current densities. As represented in Fig. 9c, the response of porous $CuCo_2O_4$ composite sheets at different applied current densities shows that the enhancement in the applied current densities resulted in the decrease in discharge time. The quasi-spherical $CuCo_2O_4$ nanoparticle also showed similar applied current density discharge time response as porous $CuCo_2O_4$ composite sheets showed (Fig. S2). From the discharge time, the specific capacity of porous $CuCo_2O_4$ composite sheet were obtained to be 449, 390, 332, 276, and 206 $C\,g^{-1}$ at 2, 4, 6, 8, and 10 $A\,g^{-1}$ current densities, respectively. The examination of the specific capacity value (Fig. 9d) clearly shows that the lowest applied current density leads to highest specific capacity and highest applied current density leads to lowest

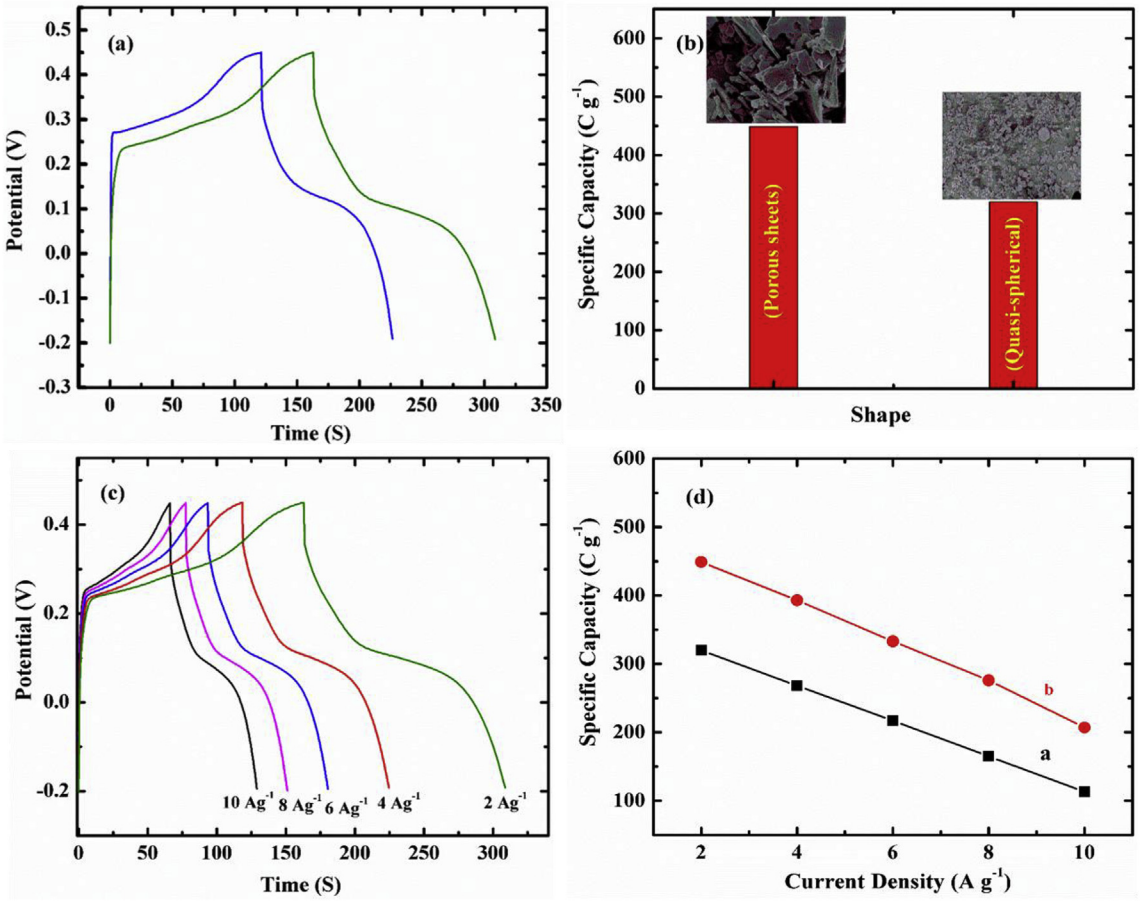

Fig. 9. (a) GCD profile of quasi-spherical $CuCo_2O_4$ nanoparticles and porous $CuCo_2O_4$ composite sheet at 2 $A\,g^{-1}$ current density. (b) Plot showing the effect of morphology on specific capacity value. (c) GCD profile of porous $CuCo_2O_4$ composite sheet based electrodes at different current density. (d) Specific capacitance versus current density of quasi-spherical $CuCo_2O_4$ nanoparticles and porous $CuCo_2O_4$ composite sheet.

Table 1
Comparison of the performance of porous $CuCo_2O_4$ sheet based supercapacitor with other reported active electrode materials.

Active materials	Specific capacity (Cg^{-1})	Current density (A g^{-1})	References
$MgCo_2O_4$ cuboids	345	1	29
$NiCo_2O_4$ flower	122.5	1	30
$ZnCo_2O_4$-PANI	398	1	31
C@MoO_2	140.4	1	32
$CuCo_2O_4$ sheets	449	2	Current work

specific capacity. The porous $CuCo_2O_4$ composite sheet based electrode delivered 206 C g^{-1} specific capacity with 46% retention even after 5 fold increase in the current density. On the other hand, the quasi-spherical $CuCo_2O_4$ nanoparticle delivered 113 C g^{-1}specific capacity with 35% retention at the same current density. The comparison of specific capacity retention % obtained on both the electrodes shows that porous $CuCo_2O_4$ composite sheet has 1.3 times higher specific capacity retention % than the quasi-spherical $CuCo_2O_4$ nanoparticle, suggesting its good rate capability and excellent performance in elevated current density situation which is important for real application. The comparison of the performance of porous $CuCo_2O_4$ composite sheet with other earlier reported active materials [40–43] reveals that porous $CuCo_2O_4$ composite sheet has better performance (Table 1). Krishnan et al. synthesized $MgCo_2O_4$ cuboids and using it as active material they achieved a specific capacity of 345 C g^{-1} at 1 A g^{-1} [40]. Jiang et al. achieved a specific capacity of 122.5 C g^{-1} at 1 A g^{-1} using $NiCo_2O_4$ flowers [41]. Recently, Omar et al. developed $ZnCo_2O_4$-PANI composite which delivered a specific capacity of 398 C g^{-1} at 1 A g^{-1} [42]. In another study, Saha et al. developed a facile method for the synthesis of C@MoO_2 hollow yolk-shell structure which delivered a specific capacity of 140.4 C g^{-1} at 1 A g^{-1} [43]. Interestingly, using porous $CuCo_2O_4$ composite sheet a highest specific capacity of 449 C g^{-1} was achieved at 2 A g^{-1}. The achievement in highest specific capacity in the current case could be attributed to the attractive porous $CuCo_2O_4$ composite sheet like morphology, large electrochemical accessible surface area, effective involvement of more available active sites in the redox reactions, faster electrolyte ion diffusion through the pores of the porous $CuCo_2O_4$ composite sheet and good structural stability [34,44].

Specific capacity retention capability of the active electrode material over a lengthy charge-discharge cycles is an important factor for real practical applications of supercapacitor, so investigation on the cyclic stability of the active electrode material is highly essential. The long term cyclic stability of the porous $CuCo_2O_4$ composite sheet based electrode was investigated for 5000 continuous charge-discharge cycles at 10 A g^{-1} current density and its response is represented in Fig. 10. As shown in Fig. 10, the initial specific capacity value increased gradually

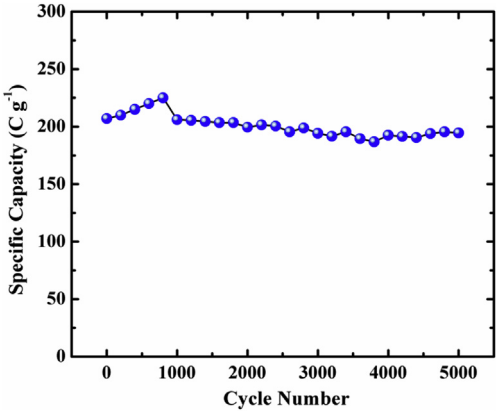

Fig. 10. Cyclic stability of porous $CuCo_2O_4$ composite sheet based electrode at 10 A g^{-1} current density for 5000 cycles.

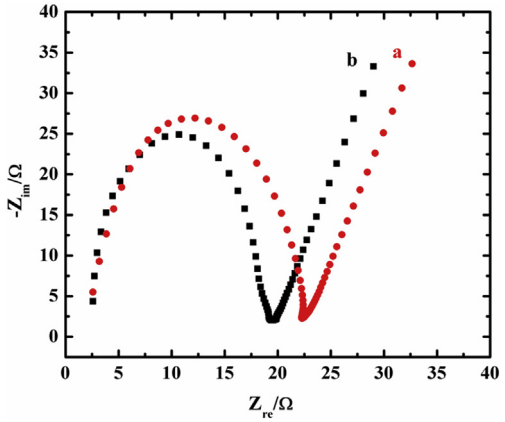

Fig. 11. Nyquist plots of (a) quasi-spherical $CuCo_2O_4$ nanoparticles and (b) porous $CuCo_2O_4$ composite sheet based electrodes.

from 207 to 225 C g^{-1} during initial 700 cycles, which could be ascribed to the activation of the material during the charge-discharge process [45,46]. After 5000 continuous GCD cycles at 10 A/g current density, the porous $CuCo_2O_4$ composite sheet based electrode successfully retained 94% of its initial specific capacity, suggesting the excellent cyclic stability of the porous $CuCo_2O_4$ composite sheet.

EIS study was performed in order to understand the ion transport properties of the quasi-spherical $CuCo_2O_4$ nanoparticle and porous $CuCo_2O_4$ composite sheet. Fig. 11 shows the Nyquist plots of quasi-spherical $CuCo_2O_4$ nanoparticle and porous $CuCo_2O_4$ sheet based electrode. The Nyquist plots of both the samples are composed of a semicircle in the high frequency region and a straight line in the low frequency region. The semicircle portion of the Nyquist plot signifies the charge transfer resistance (Rct) of the $CuCo_2O_4$ samples, which is believed to be originated from the Faradaic redox reaction of $CuCo_2O_4$. [47], whereas, the linear portion originates from the diffuse resistance of the OH^- ions from the electrolyte to the $CuCo_2O_4$ surface as well as within its pores [35]. The Rct values for quasi-spherical $CuCo_2O_4$ nanoparticle and porous $CuCo_2O_4$ composite sheet based electrode were found to be 19.7 and 16.8 Ω, respectively. The achievement in the low Rct value in the case of porous $CuCo_2O_4$ composite sheet based electrode over the quasi-spherical $CuCo_2O_4$ nanoparticle could be ascribed to the enhanced diffusion of electrolyte ions through the pores of the porous $CuCo_2O_4$ composite sheet. Since, porous $CuCo_2O_4$ composite sheet has a low Rct value than quasi-spherical $CuCo_2O_4$ nanoparticles, so, it would show better supercapacitive performance compared to the quasi-spherical $CuCo_2O_4$ nanoparticles. In a previous work, Pendashteh et al. have demonstrated that highly ordered mesoporous $CuCo_2O_4$ nanowires with a low Rct value of 3.77 Ω has enhanced supercapacitive performance over the disordered mesoporous $CuCo_2O_4$ with an Rct value of 10.6 Ω [31]. Interestingly, during the supercapacitive performance investigation, the porous $CuCo_2O_4$ composite sheet showed enhanced supercapacitive performance than the quasi-spherical $CuCo_2O_4$ nanoparticles, further supporting the linear dependence of Rct value of the $CuCo_2O_4$ with the supercapacitive performance. From the aforementioned results, it is anticipated that, $CuCo_2O_4$ with an attractive porous sheet like morphology and structural topography, high specific capacity, low Rct and excellent long-term cyclic stability is promising for use as a promising active material for the development of high performance supercapacitors.

4. Conclusions

In conclusion, a facile hydrothermal method has been developed for the synthesis of porous $CuCo_2O_4$ composite sheets and their supercapacitive performance has been demonstrated. Compared to the quasi-spherical $CuCo_2O_4$ nanoparticles, the porous $CuCo_2O_4$ sheets delivered

excellent supercapacitive performance. On the porous $CuCo_2O_4$ composite sheet based electrode a maximum specific capacity of 1037 $C\,g^{-1}$ was achieved at 5 $mV\,s^{-1}$. In addition, the porous $CuCo_2O_4$ composite sheet has excellent cyclic stability and rate capability with 94% of initial specific capacity retention after 5000 continuous charge-discharge cycles at 10 $A\,g^{-1}$. This excellent performance of porous $CuCo_2O_4$ composite sheet is attributed to its high surface area and unique morphology. The results including high specific capacity, excellent cyclic stability, reduced diffusion pathways of the electrolytes and low charge transfer resistance demonstrates that porous $CuCo_2O_4$ composite sheets are promising for use as an active material for the energy storage application.

Acknowledgements

This work was supported by KRF grant no 2017H1D3A1A01052414. This study was also supported by the Basic Research Laboratory Program (2014R1A4A1008140) and the X-mind Corps Program (2017H1D8A2030449) through the National Research Foundation (NRF) funded by the Ministry of Science and ICT of Republic of Korea.

Appendix A. Supplementary data

Supplementary data related to this article can be found at http://dx.doi.org/10.1016/j.compositesb.2018.05.028.

References

[1] Das AK, Sahoo S, Arunachalam P, Zhang S, Shim JJ. Facile synthesis of Fe_3O_4 nanorod decorated reduced graphene oxide (RGO) for supercapacitor application. RSC Adv 2016;6:107057–64.
[2] Sharma K, Maiti K, Kim NH, Hui D, Lee JH. Green synthesis of glucose-reduced graphene oxide supported Ag-Cu2O nanocomposites for the enhanced visible-light photocatalytic activity. Composites Part B 2018;138:35–44.
[3] Das AK, Kim NH, Pradhan D, Hui D, Lee JH. Electrochemical synthesis of palladium (Pd) nanorods: an efficient electrocatalyst for methanol and hydrazine electro-oxidation. Composites Part B 2018;144:11–8.
[4] Hien HV, Thanh TD, Chuong ND, Hui D, Lee JH. Hierarchical porous framework of ultrasmall PtPd alloy-integrated graphene as active and stable catalyst for ethanol oxidation. Composites Part B 2018;143:96–104.
[5] Gopalsamy K, Balamurugan J, Thanh TD, Kim NH, Hui D, Lee JH. Surfactant-free synthesis of NiPd nanoalloy/graphene bifunctional nanocomposite for fuel cell. Composites Part B 2017;114:319–27.
[6] Park OK, Kim SG, You NH, Ku BC, Hui D, Lee JH. Synthesis and properties of iodo functionalized graphene oxide/polyimide nanocomposites. Composites Part B 2014;56:365–71.
[7] Srivastava M, Uddin ME, Singh J, Kim NH, Lee JH. Preparation and characterization of self-assembled layer by layer $NiCo_2O_4$–reduced graphene oxide nanocomposite with improved electrocatalytic properties. J Alloy Comp 2014;590:266–76.
[8] Zhang C, Kuila T, Kim NH, Lee SH, Lee JH. Facile preparation of flower-like $NiCo_2O_4$/three dimensional graphene foam hybrid for high performance supercapacitor electrodes. Carbon 2015;89:328–39.
[9] Li P, Siddaramaiah, Kim NH, Heo SB, Lee JH. Novel PAAm/Laponite clay nanocomposite hydrogels with improved cationic dye adsorption behavior. Composites Part B 2008;39:756–63.
[10] Li P, Kim NH, Siddaramaiah, Lee JH. Swelling behavior of polyacrylamide/laponite clay nanocomposite hydrogels: pH-sensitive property. Composites Part B 2009;40:275–83.
[11] Khanra P, Kuila T, Bae SH, Kim NH, Lee JH. Electrochemically exfoliated graphene using 9-anthracene carboxylic acid for supercapacitor application. J Mater Chem 2012;22:24403–10.
[12] Uddin ME, Kim NH, Kuila T, Lee SH, Hui D, Lee JH. Preparation of reduced graphene oxide-NiFe2O4 nanocomposites for the electrocatalytic oxidation of hydrazine. Composites Part B 2015;79:649–59.
[13] Babu RS, Barros ALF, Maier MdA, Sampaio DdM, Balamurugan J, Lee JH. Novel polyaniline/manganese hexacyanoferrate nanoparticles on carbon fiber as binder-free electrode for flexible supercapacitors. Composites Part B 2018;143:141–7.
[14] Simon P, Gogotsi Y. Materials for electrochemical capacitors. Nat Mater 2008;7:845–54.
[15] Vijayakumar S, Lee SH, Ryu KS. Hierarchical $CuCo_2O_4$ nanobelts as a supercapacitor electrode withvhigh areal and specific capacitance. Electrochim Acta 2015;182:979–86.
[16] Zhang K, Zeng W, Zhang G, Hou S, Wang F, Wang T, Duan H. Hierarchical $CuCo_2O_4$ nanowire@$NiCo_2O_4$ nanosheet core/shell arrays for high-performance supercapacitors. RSC Adv 2015;5:69636–41.
[17] Xia X-H, Tu J-P, Zhang Y-Q, Mai Y-J, Wang X-L, Gu C-D, Zhao X-B. Freestanding Co_3O_4 nanowire array for high performance supercapacitors. RSC Adv 2012;2:1835–41.
[18] Chen D, Wang Q, Wang R, Shen G. Ternary oxide nanostructured materials for supercapacitors: a review. J Mater Chem 2015;3:10158–73.
[19] Sagu JS, Wijayantha KGU, Tahir AA. The pseudocapacitive nature of $CoFe_2O_4$ thin films. Electrochim Acta 2017;246:870–8.
[20] Zhu M, Zhang X, Zhou Y, Zhuo C, Huang J, Li S. Facile solvothermal synthesis of porous $ZnFe_2O_4$ microspheres for capacitive pseudocapacitors. RSC Adv 2015;5:39270–7.
[21] Zhu M, Meng D, Wang C, Diao G. Facile fabrication of hierarchically porous $CuFe_2O_4$ nanospheres with enhanced capacitance property. ACS Appl Mater Interfaces 2013;5:6030–7.
[22] Bandgar SB, Vadiyar MM, Ling Y-C, Chang J-Y, Han S-H, Ghule AV, Kolekar SS. Metal precursor dependent synthesis of $NiFe_2O_4$ thin films for high performance flexible symmetric supercapacitor. ACS Appl Energy Mater 2018;1:638–48.
[23] Yunyun F, Xu L, Wankun Z, Yuxuan Z, Yunhan Y, Honglin Q, Xuetang X, Fan W. Spinel $CoMn_2O_4$ nanosheet arrays grown on nickel foam for high-performance supercapacitor electrode. Appl Surf Sci 2015;357:2013–21.
[24] Wei H, Wang J, Yu L, Zhang Y, Hou D, Li T. Facile synthesis of $NiMn_2O_4$ nanosheet arrays grown on nickel foam as novel electrode materials for high-performance supercapacitor. Ceram Int 2016;42:14963–9.
[25] Guo N, Wei XQ, Deng XL, Xu XJ. Synthesis and property of spinel porous $ZnMn_2O_4$ microspheres. Appl Surf Sci 2015;356:1127–34.
[26] Hao C, Zhou S, Wang J, Wang X, Gao H, Ge C. Preparation of hierarchical spinel $NiCo_2O_4$ nanowires for high performance supercapacitors. Ind Eng Chem Res 2018;57:2517–25.
[27] Cui L, Huang L, Ji M, Wang Y, Shi H, Zuo Y, Kang S. High-performance $MgCo_2O_4$ nanocone arrays grown on three dimensional nickel foams: preparation and application as binder-free electrode for pseudo-supercapacitor. J Power Sources 2016;333:118–24.
[28] Gai Y, Shang Y, Gong L, Su L, Hao L, Dong F, Li J. A self-template synthesis of porous $ZnCo_2O_4$ microspheres for high-performance quasi-solid state asymmetric supercapacitors. RSC Adv 2017;7:1038–44.
[29] Zhu B, Tang S, Vongehr S, Xie H, Zhu J, Meng X. $FeCo_2O_4$ submicron-tube arrays grown on Ni foam as high rate-capability and cycling-stability electrodes allowing superior energy and power densities with symmetric supercapacitors. Chem Commun 2016;52:2624–7.
[30] Sahoo S, Naik KK, Rout CS. Electrodeposition of spinel $MnCo_2O_4$ nanosheets for supercapacitor applications. Nanotechnology 2015;26:455401.
[31] Pendashteh A, Moosavifard SE, Rahmanifar MS, Wang Y, El-Kady MF, Kaner RB. Mousavi MF, Highly ordered mesoporous $CuCo_2O_4$ nanowires, a promising solution for high- performance supercapacitors. Chem Mater 2015;27:3919–26.
[32] Cheng J, Yan H, Lu Y, Qiu K, Hou X, Xu J, Han L, Liu X, Kim J-K, Luo Y. Mesoporous $CuCo_2O_4$ nanograsses as multifunctional electrodes for supercapacitors and electrocatalysts. J Mater Chem 2015;3:9769–76.
[33] Sharma Y, Sharma N, SubbaRao GV, Chowdari BVR. Lithium recycling behaviour of nano-phase-$CuCo_2O_4$ as anode for lithium-ion batteries. J Power Sources 2007;173:495–501.
[34] Wang Q, Chen D, Zhang D. Electrospun porous $CuCo_2O_4$ nanowire network electrode for asymmetric supercapacitors. RSC Adv 2015;5:96448–54.
[35] Pendashteh A, Rahmanifar MS, Kaner RB, Mousavi MF. Facile synthesis of nanostructured $CuCo_2O_4$ as a novel electrode material for high-rate supercapacitors. Chem Commun 2014;50:1972–5.
[36] Nakhowong R, Chueachot R. Synthesis and magnetic properties of copper cobaltite ($CuCo_2O_4$) fibers by electrospinning. J Alloy Comp 2017;715:390–6.
[37] Prasad R, Singh PS. Low temperature complete combustion of a lean mixture of LPG emissions over cobaltite catalysts. Catal Sci Technol 2013;3:3223–33.
[38] Grosso D, Illia G, Crepaldi EL, Charleux B, Sanchez C. Nanocrystalline transition-metal oxide spheres with controlled multi-scale porosity. Adv Funct Mater 2003;13:37–42.
[39] Vijayakumar S, Nagamuthu S, Ryu K-S. $CuCo_2O_4$ flowers/Ni-foam architecture as a battery type positive electrode for high performance hybrid supercapacitor applications. Electrochim Acta 2017;238:99–106.
[40] Krishnan SG, Harilal M, Misnon II, Reddy MV, Adams S, Jose R. Effect of processing parameters on the charge storage properties of $MgCo_2O_4$ electrodes. Ceram Int 2017;43:12270–9.
[41] Jiang W, Hu F, Yan Q, Wu X. Investigation on electrochemical behaviors of $NiCo_2O_4$ battery-type supercapacitor electrodes: the role of an aqueous electrolyte. Inorg Chem Front 2017;4:1642–8.
[42] Omar FS, Numan A, Duraisamy N, Bashir S, Ramesh K, Ramesh S. A promising binary nanocomposite of zinc cobaltite intercalated with polyaniline for supercapacitor and hydrazine sensor. J Alloy Comp 2017;716:96–105.
[43] Saha A, Mondal A, Maiti S, Ghosh SC, Mahanty S, Panda AB. A facile method for the synthesis of a C@MoO_2 hollow yolk–shell structure and its electrochemical properties as a faradaic electrode. Mater Chem Front 2017;1:1585–93.
[44] Meher SK, Rao GR. Ultralayered Co_3O_4 for high-performance supercapacitor applications. J Phys Chem C 2011;115:15646–54.
[45] Tang X, Li H, Liu Z-H, Yang Z, Wang Z. Preparation and capacitive property of manganese oxide nanobelt bundles with birnessite-type structure. J Power Sources 2011;196:855–9.
[46] Nagamuthu S, Vijayakumar S, Muralidharan G. Synthesis of Mn_3O_4/Amorphous carbon nanoparticles as electrode material for high performance supercapacitor applications. Energy Fuels 2013;27:3508–15.
[47] Cheng J, Lu Y, Qiu K, Yan H, Xu LH, Luo J, Kim J-K, Luo Y. Hierarchical core/shell $NiCo_2O_4$@$NiCo_2O_4$ nanocactus arrays with dual-functionalities for high performance supercapacitors and Li-ion batteries. Sci Rep 2015;5:12099.